A&A 609, A134 (2018)
DOI: 10.1051/0004-6361/201730842

Astronomy & Astrophysics

The Carnegie Supernova Project I

Photometry data release of low-redshift stripped-envelope supernovae[⋆,⋆⋆]

M. D. Stritzinger[1,2], J. P. Anderson[3], C. Contreras[2,1], E. Heinrich-Josties[4,5], N. Morrell[2], M. M. Phillips[2], J. Anais[2], L. Boldt[2], L. Busta[6], C. R. Burns[5], A. Campillay[2], C. Corco[7,2], S. Castellon[2], G. Folatelli[8,2], C. González[2], S. Holmbo[1], E. Y. Hsiao[9,1,2], W. Krzeminski[10,2,†], F. Salgado[11,2], J. Serón[7,2], S. Torres-Robledo[12,2], W. L. Freedman[13,5], M. Hamuy[14,2], K. Krisciunas[15], B. F. Madore[5,16], S. E. Persson[5], M. Roth[2], N. B. Suntzeff[15], F. Taddia[17], W. Li[18,†], and A. V. Filippenko[18,19]

[1] Department of Physics and Astronomy, Aarhus University, Ny Munkegade 120, 8000 Aarhus C, Denmark
e-mail: max@phys.au.dk
[2] Carnegie Observatories, Las Campanas Observatory, Casilla 601, La Serena, Chile
[3] European Southern Observatory, Alonso de Cordova 3107, Vitacura, Casilla 19001, Santiago, Chile
[4] Las Cumbres Observatory, 6740 Cortona Dr., Suite 102, Goleta, CA 93117, USA
[5] Observatories of the Carnegie Institution for Science, 813 Santa Barbara St., Pasadena, CA 91101, USA
[6] Institut für Astro- and Particle Physics, University of Innsbruck, 6020 Innsbruck, Austria
[7] Cerro Tololo Inter-American Observatory, Casilla 603, La Serena, Chile
[8] Facultad de Ciencias Astronómicas y Geofísicas, Universidad Nacional de La Plata, Paseo del Bosque S/N, B1900FWA La Plata, Argentina
[9] Department of Physics, Florida State University, 77 Chieftain Way, Tallahassee, FL 32306, USA
[10] N. Copernicus Astronomical Center, ul. Bartycka 18, 00-716 Warszawa, Poland
[11] Leiden Observatory, Leiden University, PO Box 9513, 2300 RA Leiden, The Netherlands
[12] SOAR Telescope, Casilla 603, La Serena, Chile
[13] Department of Astronomy & Astrophysics, University of Chicago, 5640 South Ellis Avenue, Chicago, IL 60637, USA
[14] Departamento de Astronomia, Universidad de Chile, Casilla 36D, Santiago, Chile
[15] George P. and Cynthia Woods Mitchell Institute for Fundamental Physics and Astronomy, Department of Physics and Astronomy, Texas A&M University, College Station, TX 77843, USA
[16] Infrared Processing and Analysis Center, Caltech/Jet Propulsion Laboratory, Pasadena, CA 91125, USA
[17] The Oskar Klein Centre, Department of Astronomy, Stockholm University, AlbaNova, 10691 Stockholm, Sweden
[18] Department of Astronomy, University of California, Berkeley, CA 94720-3411, USA
[19] Miller Senior Fellow, Miller Institute for Basic Research in Science, University of California, Berkeley, CA 94720, USA

Received 22 March 2017 / Accepted 9 August 2017

ABSTRACT

The first phase of the Carnegie Supernova Project (CSP-I) was a dedicated supernova follow-up program based at the Las Campanas Observatory that collected science data of young, low-redshift supernovae between 2004 and 2009. Presented in this paper is the CSP-I photometric data release of low-redshift stripped-envelope core-collapse supernovae. The data consist of optical (*uBgVri*) photometry of 34 objects, with a subset of 26 having near-infrared (*YJH*) photometry. Twenty objects have optical pre-maximum coverage with a subset of 12 beginning at least five days prior to the epoch of *B*-band maximum brightness. In the near-infrared, 17 objects have pre-maximum observations with a subset of 14 beginning at least five days prior to the epoch of *J*-band maximum brightness. Analysis of this photometric data release is presented in companion papers focusing on techniques to estimate host-galaxy extinction and the light-curve and progenitor star properties of the sample. The analysis of an accompanying visual-wavelength spectroscopy sample of ~150 spectra will be the subject of a future paper.

Key words. supernovae: general

1. Introduction

The first phase of the Carnegie Supernova Project (CSP-I; Hamuy et al. 2006) was an observational supernova (SN) follow-up program that collected data on most varieties of supernovae (SNe) between 2004 to 2009, mainly using facilities located at the Las Campanas Observatory (LCO). A key goal of the CSP-I was to build a well-observed sample of stripped-envelope (SE) core-collapse SNe in a stable and well-characterized photometric system. SE SNe (which we define as Type IIb, Type Ib, Type Ic, and Type Ic SNe-BL, collectively) are thought to be linked to the death of massive stars which experience significant mass loss over their evolutionary lifetimes. Contemporary

⋆ Based on observations collected at Las Campanas Observatory.
⋆⋆ Tables 2–8 are only available at the CDS via anonymous ftp to cdsarc.u-strasbg.fr (130.79.128.5) or via http://cdsarc.u-strasbg.fr/viz-bin/qcat?J/A+A/609/A134
† Deceased

estimates from a volume-limited sample obtained during the Lick Observatory Supernova Search (LOSS; Filippenko et al. 2001; Filippenko 2005) with the Katzman Automatic Imaging Telescope suggest that SE SNe account for ∼26% of the overall SN rate in the local Universe (Li et al. 2011).

The presence of residual hydrogen and helium maintained by the progenitor at the time of explosion, and how it manifests itself in the optical spectrum of the SN, provides the basis for today's spectral classification scheme of SE SNe (see, e.g., Filippenko 1997; Gal-Yam 2016; Liu et al. 2017; Modjaz et al. 2016; Shivvers et al. 2017; Prentice & Mazzali 2017). Based mostly on historical observations, the current classification system has become somewhat ambiguous with the advent of detailed spectroscopic follow-up campaigns of low-redshift objects. SE SNe are grouped into subtypes based on spectroscopic signatures ranging from helium rich with traces of hydrogen (Type IIb), to helium rich with no traces of hydrogen (Type Ib), to helium and hydrogen deficient (Type Ic). Early-time spectra of SNe IIb exhibit prevalent P Cygni Balmer lines akin to normal hydrogen-rich SNe II; however, by several weeks past explosion their spectrum experiences a metamorphosis and subsequently resembles that of a classical SN Ib. Given these unique characteristics, such transitional objects are designated SNe IIb, of which SN 1987K was the first known example (Filippenko 1988) and SN 1993J is the prototypical example (e.g., Filippenko et al. 1993; Swartz et al. 1993). In both SNe IIb and SNe Ib, He I features tend to dominate the spectrum around a month past explosion (Harkness et al. 1987; Matheson et al. 2001). The current classification scheme therefore reflects to first order the mass-loss history of the progenitors with increased stripping driving the SN IIb → SN Ib → SN Ic spectroscopic sequence.

Initially, SNe Ib and Ic garnered relatively little interest within the astronomical community. This changed in 1998, when the gamma-ray burst (GRB) 980425 was demonstrated to be linked to the peculiar Type Ic SN 1998bw (Galama et al. 1998; Iwamoto et al. 1998), which showed very broad spectral lines. Five years later the GRB–SN connection was firmly established (Hjorth et al. 2003; Matheson et al. 2003; Stanek et al. 2003; Mazzali et al. 2006). In each instance of a GRB–SN association, the underlying "relativistic" SN exhibited broad absorption features indicative of expansion velocities in excess of $\sim$30 000 km s^{-1}, and explosion energies of $\gtrsim 10^{52}$ erg. These events are thought to be powered by a central engine or a relativistic outflow, and constitute only ∼1% of the total SE SN population.

For comparison, the vast majority of *normal* SE SNe typically exhibit expansion velocities of <15 000 km s^{-1}, and kinetic energies of $\sim 10^{51}$ erg. Interestingly, an additional subtype has been identified that shows enhanced expansion velocities ($\sim$20 000 km s^{-1}), but whose kinetic energies are equivalent to those of normal SE SNe. Given their spectral characteristics these objects are commonly referred to as BL (broad-lined). SN 2002ap serves as the prototypical SN Ic-BL (Mazzali et al. 2002; Foley et al. 2003), while SN 2003bg is the first identified SN IIb-BL (Hamuy et al. 2009; Mazzali et al. 2009). Finally, a handful of peculiar events have been studied that do not follow the light curve and/or spectral templates garnered from the normal SE SN population. These objects may, as in the case of SN 2005bf (see light curves below), exhibit bizarre double-humped light curves (see also Anupama et al. 2005; Tominaga et al. 2005; Folatelli et al. 2006), or in the instances of SN 2001co, SN 2005E, and SN 2005cz, enhanced calcium abundances (Filippenko et al. 2003; Perets et al. 2010; Kawabata et al. 2010).

Although the identity of SE SN progenitors has long remained rather inconclusive, the early-time light-curve evolution of the Type IIb SN 1993J exhibited an initial declining phase right after its explosion, followed by a rise to peak luminosity driven by the decay of ^{56}Ni within several weeks (e.g., van Driel et al. 1993; Richmond et al. 1994). This light-curve evolution is indicative of a massive progenitor that explodes via core collapse. A similar early-time bump was also detected in the Type Ib SN 1999ex (Stritzinger et al. 2002), and in recent years early bumps have been used to constrain the radius of the progenitor star in a number of cases, such as SN 2008D (Chevalier & Fransson 2008; Bersten et al. 2013), SN 2011dh (Arcavi et al. 2011; Soderberg et al 2012; Bersten et al. 2012), SN 2011fu (Kumar et al. 2013), SN 2011hs (Bufano et al. 2014), SN 2013df (Morales-Garoffolo et al. 2014), and SN 2016gkg (Tartaglia et al. 2017; Arcavi et al. 2017).

Efforts to model SE SNe usually assume progenitor systems encompassing either single massive (>20 $M_\odot$) Wolf-Rayet stars, or moderately massive (8–25 $M_\odot$) stars in binary systems (for a review see Yoon 2015, and references therein). Stars within the former scenario are thought to shed the majority of their hydrogen-rich envelopes via line-driven winds, while stars within the latter scenario are thought to lose their hydrogen-rich envelopes through Roche-lobe overflow (RLOF) to their companions and/or during common-envelope evolution. Finally, rotationally induced mixing has been suggested to play a role in growing the core mass at the expense of the envelope mass (see, e.g., Langer 2012). In the near future, robust constraints on the expelled gas will be possible by studying spectral features associated with circumstellar material flash-ionized by ultraviolet light from the SN shock breakout in very early spectra, within one day or a few days of explosion (e.g., Gal-Yam et al. 2014; Shivvers et al. 2015; Yaron et al. 2017).

Despite the heroic efforts to model SE SNe, the evolutionary scenarios of the various spectroscopically defined subtypes such as SN IIb, Ib, Ic, and Ic-BL are not completely understood. Ideally, the putative detection of the progenitor star in pre-explosion images (Smartt 2009; Eldridge et al. 2013) provides the gold standard; however, these opportunities are rare, often controversial, and to date exist for only a handful of events including the Type IIb SN 1993J (Aldering et al. 1995; Cohen et al. 1995), SN 2008ax (Li 2008; Crockett et al. 2008), SN 2011dh (Maund et al. 2011; Van Dyk et al. 2011; Ergon et al. 2014), iPTF 13bvn (Cao et al. 2013; Groh et al. 2013), and SN 2013df (Van Dyk et al. 2014).

An alternative avenue is to constrain the nature of SE SN progenitors by observing the site of the explosion with the *Hubble* Space Telescope (HST) hundreds of days to a few years after the SN exploded. For example, deep HST imaging of iPTF 13bvn indicates a late-time (+740 days) SN brightness below that measured for the candidate progenitor star in pre-explosion HST images (Folatelli et al. 2016; Eldridge & Maund 2016). Folatelli et al. (2016) assert that with these observations, the characterization of the progenitor star is currently inconclusive, and the progenitor's companion was either a late-O star or suffers from significant extinction produced by newly formed dust. On the other hand, Eldridge & Maund (2016) suggest (from the same data) that the companion star had a mass of ∼10 $M_\odot$ or less, and that the progenitor itself was possibly a 10–12 $M_\odot$ helium giant star.

Similarly, HST images of the Type IIb SN 2011dh obtained ∼1160 days after explosion reveal a blue source that may have been the companion star (Folatelli et al. 2014) to

a yellow supergiant prior to its death (Bersten et al. 2012; Benvenuto et al. 2013), though this interpretation has been challenged (Maund et al. 2015). Of course, these cases follow in the footsteps of the well-studied Type IIb SN 1993J, whose massive companion was identified in late-phase HST imaging (Maund et al. 2004; Fox et al. 2014).

Taken together, the current literature on SE SNe suggests that at least a portion of these cosmic explosions arise from binary-star systems. Contemporary studies of hot and cool, single, massive stars indicate mass-loss rates ∼2–10 times less than those typically adopted in late-stage stellar evolutionary models (Puls et al. 2008, and references therein). When considering revised mass-loss rates, in combination with the observed SN rates, one obtains rather strong (albeit indirect) constraints that the majority of SE SN progenitors are moderately massive stars in binary systems (Smith et al. 2011). Moreover, the implied lower mass-loss rates suggest that single massive stars require more efficient mass-stripping mechanisms in order to shed their outer hydrogen and helium layers prior to exploding. Potential mechanisms that have been suggested to drive enhanced mass loss include pulsation-driven superwinds (e.g., Yoon & Cantiello 2010) and episodic luminous blue variable (LBV) outbursts during the pre-SN evolution (e.g., Smith & Owocki 2006; Smith et al. 2011; Vink 2011).

Given the lack of constraints on SE SN progenitor properties from direct detection methods, investigations of their local environments have been pursued. Anderson et al. (2012) found that SNe Ic are projected on regions of higher star-formation intensity within host galaxies than both SNe Ib and SNe II, and suggested this implies higher-mass progenitors for the SNe Ic (with an only marginal difference of environment found between the SNe Ib and SNe IIb). Host H II region metallicity studies of SE SNe have attempted to probe progenitor metallicity differences; however, results have thus far been inconclusive as to whether metallicity inferred from line diagnostics (e.g., Pettini & Pagel 2004) significantly affects the final outcome of progenitor stars through the role of line-driven winds; see Anderson et al. (2010), Modjaz et al. (2011), Leloudas et al. (2011), and Sanders et al. (2012). A compilation of all literature measurements is presented in Galbany et al. (2016). Most recently, Graur et al. (2017a) revisited the LOSS sample in order to search for correlations between SN rates and galaxy properties, while Graur et al. (2017b) compare the relative rates of different SN types to the masses of the host galaxies.

Until recently, the literature sample of SE SNe with multiband light curves was rather limited, with only a handful of objects having been well studied. However, with an enhanced interest in this SN class and the advent of monitoring programs, detailed studies of nearby objects are more common. For example, Drout et al. (2011) presented V- and R-band light curves of 25 SE SNe. Combined with the best-observed objects in the literature, they were able to study a statistically significant sample. Most recently, Bianco et al. (2014) and Taddia et al. (2015) have presented expanded sets of multiband SE SN light curves obtained by the CfA Supernova Group and the SDSS-II SN survey, respectively, while detailed studies of literature-based samples have been presented by Cano (2013), Lyman et al. (2016), and Prentice et al. (2016). These papers are discussed in a companion paper (Taddia et al. 2018), which also contains a detailed study of the CSP-I SE SN light-curve sample. It includes the estimation of key explosion parameters by comparing best-fit analytical and hydrodynamical modeled bolometric light curves to bolometric light curves constructed from the broad-band observations presented here. In short, consistent with previously studied SE SN samples, we estimate the ^{56}Ni abundance, the ejecta mass ($M_{\rm ej}$), and the explosion energy (E_K). Quantitatively, for the majority of normal SE SNe, these parameters range from ∼0.03 to 0.38 $M_\odot$ of radioactive ^{56}Ni, ∼1.1 to 6.2 $M_\odot$ of $M_{\rm ej}$, and (excluding SNe Ic-BL) E_K between 0.25 × 10^{51} and 3.0 × 10^{51} erg (Taddia et al. 2018).

Continued advances in the understanding of SE SNe will come from the detailed studies of *homogeneous* samples. New datasets will enable (i) improved methods to estimate host-galaxy dust extinction; (ii) the construction of accurate ultraviolet–optical–near-infrared (UVOIR) bolometric light curves useful for model comparisons; and (iii) better knowledge of their spectroscopic properties. Furthermore, with the advent of new, high-cadence surveys, observations of SE SNe discovered just after explosion combined with improved models (e.g., Bersten et al. 2012; Nakar & Piro 2014; Piro 2015; Sapir & Waxman 2017; Piro et al. 2017) will provide better constraints on the progenitors and their pre-SN evolution.

In this paper, we present photometry of the CSP-I sample of low-redshift SE SNe. Our dataset consists of optical light curves of 34 SE SNe, with a subset of 26 objects also having accompanying near-infrared (NIR) light curves. Three of these objects – SN 2005bf (Folatelli et al. 2006), SN 2007Y (Stritzinger et al. 2009), and SN 2009bb (Pignata et al. 2011) – have been the subject of individual case studies by the CSP-I. The photometry reported here of these objects supersedes what has been previously published, and is based on definitive color and extinction coefficient terms characterizing the CSP-I natural photometric system as presented by Krisciunas et al. (2017). These updates have minimal differences compared to the originally published photometry and in no way affect any results previously presented.

This paper is accompanied by three companion papers. In Stritzinger et al. (2018), our SE SN photometry is used to devise robust methods to estimate host-galaxy extinction. Taddia et al. (2018) use the photometry to construct UVOIR bolometric light curves which are modeled to estimate key explosion parameters. Finally, Holmbo et al. (in prep.) present a detailed study of the accompanying sample of visual-wavelength spectroscopy.

2. The sample

The CSP-I performed follow-up observations on all varieties of southern and equatorial SNe discovered by both professional and amateur-led search programs. The general restrictions considered to place an object in the follow-up queue were its temporal phase and brightness. Selected targets were thought to have been discovered prior to or just after maximum luminosity and were estimated to reach peak apparent brightness no fainter than 18 mag. Owing to these observational guidelines and the methods used by the search programs that discovered the SNe, the majority of the sample is located rather nearby (redshift $z \leq 0.03$). This is demonstrated in the redshift distribution presented as a stacked histogram in Fig. 1, where only two objects within the sample are located at $z > 0.035$. Given that the majority of the CSP-I SE SNe were discovered by targeted surveys, the sample is biased, as the targeted search strategy leads to an underrepresentation of segments of the population, particularly objects located in faint, metal-poor galaxies (Arcavi et al. 2010).

General properties of each of the objects in the CSP-I sample are summarized in Table 1, including (i) their J2000.0 coordinates; (ii) host-galaxy type and morphology as provided by

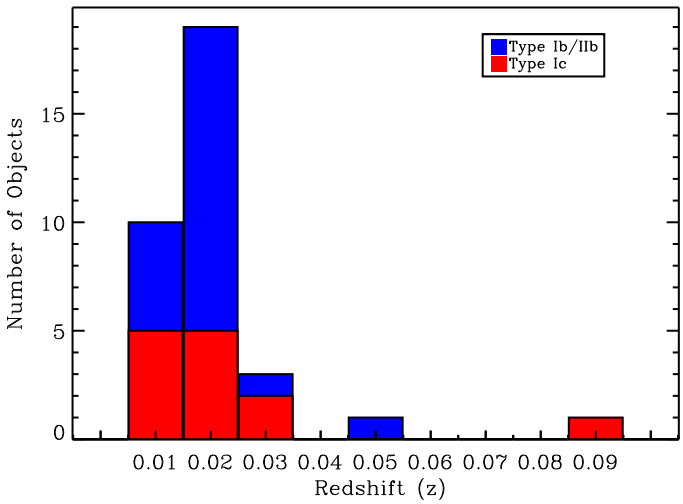

Fig. 1. Stacked histogram of the redshift distribution of SN Ib/IIb (blue) and SN Ic (red) observed by the CSP-I.

NED; (iii) the heliocentric redshift as listed in NED or as determined by our own spectral analysis; (iv) a reference to the reported discovery; (v) the group or individual(s) credited with the discovery; (vi) the spectral classification of each object; (vii) the phase range of the obtained spectra; (viii) and an estimate of the epoch of *B*-band maximum brightness (see below).

Spectral classification was made through the careful inspection of all available spectra (see Holmbo et al., in prep.). The decision to classify a particular object as a SN IIb or a SN Ib was based on the strength of Hα and the presence and strength of any conspicuous He I absorption features. If Hα was prominent while He I was either weak or absent, a SN IIb classification was preferred, while weak Hα and conspicuous He I absorption yielded a SN Ib subtyping. However, these criteria can be misleading, as they are highly dependent on the temporal phase of the earliest spectrum used to make the classification (Stritzinger et al. 2009; Chornock et al. 2011; Milisavljevic et al. 2013; Shivvers et al. 2017). For example, it is possible that an object classified as a SN Ib based on a spectrum taken at maximum brightness or even two weeks earlier could have appeared as a SN IIb soon after explosion. The temporal phases of the spectroscopic sample listed in Table 1 indicate there are a few such cases: SN 2004ew, SN 2006ep, and SN 2008gc. Similarly, attempting to make a distinction between some SNe Ib and SNe Ic was not always clear, and (as previously mentioned) highly dependent on the number of spectra and the breadth of the temporal phase covered. This includes SN 2005em, SN 2007ag, and SN 2009dt, whose spectroscopic coverage does not extend sufficiently far past maximum brightness to ensure the lack of He I features. With these caveats in mind, Table 1 includes our best spectral classifications for each object within the sample, and we note that these classifications agree with best-fit matches made with SNID (SuperNova IDentification; Blondin & Tonry 2007) using both standard and expanded template sets (Liu et al. 2014). The final tally is as follows: 10 SNe IIb, 11 SNe Ib, 11 SNe Ic, and 2 SNe Ic-BL.

Figure A.1 contains a single *V*-band image for each of the SE SNe in the CSP-I obtained with the *Henrietta Swope* 1 m telescope at Las Campanas Observatory (LCO). Each image is oriented such that the SN, marked with a blue circle, is located at the center of the field. In addition, visible local sequence stars are indicated with red squares.

3. Optical and NIR passbands

The majority of imaging of the CSP-I SE SN sample was performed by the LCO Swope 1 m telescope equipped with a direct CCD camera named after its detector "SITe3" and a NIR imager specifically built for the CSP-I named "RetroCam". A significant amount of NIR imaging was also performed by the LCO *Irénée du Pont* 2.5 m telescope equipped with the Wide Field IR Camera (WIRC), and a small amount of optical imaging was performed with the facility Tek5 CCD camera using the same filter set used with the Swope+SITe3 telescope. Readers are referred to Hamuy et al. (2006) for details on CSP-I instrumental setups and observing procedures.

The CSP-I carried out a detailed photometric calibration program in order to accurately measure the Swope+SITe3 and Swope+RetroCam and the du Pont+WIRC system (telescope+instrument+filters) response functions. Unfortunately no scans were made for the du Pont+Tek5, however, after some detailed experimentation we have found that the du Pont+Tek5 system response functions are in complete agreement with the Swope+SIT3 system response functions (see Krisciunas et al. 2017).

A detailed account of the experimental setup used to conduct the measurements of the system response functions is presented by Rheault et al. (2010), and the optical (*uBgVri* band) system response functions are presented by Stritzinger et al. (2011). NIR (*YJH* band) system response functions are presented here, and in a companion paper presenting the final CSP-I Type Ia supernova light-curve data release (Krisciunas et al. 2017)[1]. Here we provide a brief overview of the instrumental calibration project and present definitive system response functions used to observe the CSP-I SE SN sample[2].

The experimental setup consists of an appropriate light source connected to a monochromator that allows one to step through wavelength in a narrow bandwidth of light (see Stritzinger et al. 2011, for detailed specifics). The light is fed from the monochromator through a fiber optic bundle and projected onto a highly reflective flat-field screen. Light entering the telescope is measured by a system of calibrated germanium (optical: 2500–10 000 Å) and InGaAs (NIR: 8000–16 500 Å) photodiodes placed behind the secondary mirror. Exposures are taken with the facility instrument and the resulting signal is compared to the incoming signal measured by the photodiodes. This is a relative measurement that yields the system response function. The process is performed in a scanning manner as the monochromator is used to step through wavelength.

Scanning was performed over the course of two calibration runs and each passband was scanned a minimum of two times per run. The repeatability of the measured optical system response function indicates the relative throughputs were measured with a precision of 1% or less (see Stritzinger et al. 2011), while repeatable scanning of the NIR system response functions indicate relative throughputs were measured with a precision of 2–3%.

Plotted in Fig. 2 are the scanned optical (top panel) and NIR (bottom panel) system response functions used to obtain data of the CSP-I SE SN sample. The scanned system response

[1] The final CSP-I SNe Ia data release paper contains complete details concerning our natural photometric systems including robust measurements of extinction-term coefficients, color-term coefficients, and photometric zero-points.

[2] Optical/NIR system response functions are available in ASCII format on the CSP-I webpage located here: http://csp.obs.carnegiescience.edu/

Table 1. General properties of 34 Type Ibc and Type IIb supernovae.

SN	α(2000)	δ(2000)	Host	Morphology[a]	$z_{\rm helio}$[b]	Discovery	Discovery group[c]	Spectral ID	Phase range	$T(\mathrm{B})_{\rm max}$[d]
2004ew	02:05:06.17	−05:06:31.6	ESO 153−G17	SAB(r)bc	0.0218	CBET 96	Monard	Ib	+13 ··· +69	3277.79 ± 2.08‡
2004ex	00:38:10.17	+02:43:16.9	NGC 182	SAB(rs)a pec	0.0176	IAUC 8418	Trondal & Schwartz	IIb	−3 ··· +42	3306.67 ± 0.06
2004fe	00:30:11.27	+02:05:23.5	NGC 132	SAB(s)bc	0.0179	IAUC 8425	LOSS	Ic	+10 ··· +36	3316.80 ± 0.04
2004ff	04:58:46.19	−21:34:12.0	ESO 552−G40	SB(s)ab pec	0.0227	IAUC 8425	LOSS	IIb	+14 ··· +31	3312.66 ± 0.27
2004gq	05:12:04.81	−15:40:54.2	NGC 1832	SB(r)bc	0.0065	IAUC 8452	LOSS	Ib	−5 ··· +23	3357.92 ± 0.02
2004gt	12:01:50.37	−18:52:12.7	NGC 4038	SB(s)m pec	0.0055	IAUC 8454	Monard	Ic	−1 ··· +50	3360.07 ± 0.76
2004gv	02:13:37.42	−00:43:05.8	NGC 856	(R)SA(rs)0/a	0.0199	IAUC 8454	Chen	Ib	−7 ··· −7	3365.28 ± 0.27
2005Q	01:30:03.51	−42:40:48.4	ESO 244−G31	SA(rs)c	0.0224	CBET 106	Monard	IIb	+0 ··· +8	3406.17 ± 0.23
2005aw	19 15 17.44	−54:08:24.9	IC 4837A	SA(s)b:sp	0.0095	CBET 127	Jacques & Pimentel	Ic	+7 ··· +23	3457.44 ± 1.71‡
2005bf	10:23:57.27	−03:11:28.6	MCG +00−27−05	SB(r)b	0.0189	IAUC 8507	Monard	Ib	−7 ··· +53	3474.95 ± 0.12
2005bj	16:49:44.74	+17:51:48.7	MCG +03−43−5	G	0.0222	CBET 137	Boles	IIb	−1 ··· +2	3472.26 ± 1.44‡
2005em	03:13:47.71	−00:14:37.0	IC 307	G/(R)SB(r)a pec	0.0260	IAUC 8604	Boles	Ic	+3 ··· +3	3648.01 ± 3.41‡
2006T	09:54:30.21	−25:42:29.3	NGC 3054	SAB(r)bc	0.0081	CBET 385	Monard	IIb	+0 ··· +71	3779.62 ± 0.01
2006ba	09:43:13.40	−09:36:53.0	NGC 2980	SAB(s)c?	0.0191	CBET 443	Monard	IIb	−6 ··· +19	3820.90 ± 1.44‡
2006bf	12:58:50.68	+09:39:30.1	UGC 8093	S	0.0239	IAUC 8693	Puckett	IIb	+1 ··· +4	3817.79 ± 2.08‡
2006ep	00:41:24.88	+25:29:46.7	NGC 214	SAB(r)c	0.0151	CBET 609	LOSS/Itagaki	Ib	+19 ··· +34	3985.49 ± 0.60
2006fo	02:32:38.89	+00:37:03.0	UGC 02019	Sab	0.0207	CBET 624	SDSS-II	Ib	+0 ··· +17	4003.11 ± 1.45‡
2006ir	23:04:35.68	+07:36:21.5	KUG 2302+073	···	0.0200	CBET 658	SNFactory	Ic	+2 ··· +26	3999.49 ± 2.08‡
2006lc	22:44:24.48	−00:09:53.5	NGC 7364	S0/a pec	0.0162	CBET 688	SDSS-II	Ib	+1 ··· +1	4041.23 ± 0.04
2007C	13:08:49.30	−06:47:01.0	NGC 4981	SAB(r)bc	0.0056	CBET 798	Itagaki	Ib	+3 ··· +97	4114.95 ± 1.44‡
2007Y	03:02:35.92	−22:53:50.1	NGC 1187	SB(r)c	0.0046	CBET 845	Mondard	Ib	−13 ··· +40	4163.06 ± 0.01
2007ag	10:01:35.99	+21:36:42.0	UGC 5392	Sd	0.0207	CBET 868	Puckett	Ic	−1 ··· +2	4163.62 ± 3.00‡
2007hn	21:02:46.85	−04:05:25.2	2MASX J21024677−0405233	···	0.0273†	CBET 1050	SNFactory	Ic	+12 ··· +60	4353.81 ± 1.45‡
2007kj	00:01:19.58	+13:06:30.6	NGC 7803	S0/a	0.0179	CBET 1092	Itagaki	Ib	−4 ··· +41	4381.47 ± 0.18
2007rz	04:31:10.84	+07:37:51.5	NGC 1590	Pec	0.0130	CBET 1158	LOSS	Ic	−1 ··· +24	4437.49 ± 2.08‡
2008aq	12:50:30.42	−10:52:01.4	MCG−02−33−020	SB(s)m	0.0080	CBET 1271	LOSS	IIb	−2 ··· +311	4531.27 ± 0.03
2008gc	02:10:36.63	−53:45:59.5	anonymous	···	0.0492†	CBET 1529	CHASE	Ib	+14 ··· +29	4746.99 ± 2.08‡
2008hh	01:26:03.65	+11:26:26.5	IC 112	Sdm	0.0194	CBET 1575	Puckett	Ic	+1 ··· +31	4791.49 ± 2.08‡
2009K	04:36:36.77	−00:08:35.6	NGC 1620	SAB(rs)bc	0.0117	CBET 1663	CHASE	IIb	−19 ··· +285	4867.42 ± 0.02
2009Z	14:01:53.61	−01:20:30.2	2dFGRS N271Z016	dI	0.0251	CBET 1685	LOSS	IIb	−6 ··· +42	4877.13 ± 0.20
2009bb	10:31:33.87	−39:57:30.0	NGC 3278	SA(s)c?	0.0099	CBET 1731	CHASE	Ic-BL	−1 ··· +310	4920.01 ± 0.03
2009ca	21:26:22.20	−40:51:48.6	···	···	0.0956†	CBET 1750	CHASE	Ic-BL	+1 ··· +16	4926.19 ± 2.08‡
2009dp	20:26:52.69	−18:37:04.2	NGC 6912	SB(s)c	0.0232	CBET 1779	Monard	Ic	+4 ··· +37	4949.89 ± 2.08‡
2009dt	22:10:09.27	−36:05:42.6	IC 5169	(R)SAB0$^+$(r) pec	0.0104	CBET 1785	CHASE	Ic	−6 ··· −6	4958.13 ± 1.47‡

Notes. [a] Morphologies are as listed in the NASA/IPAC Extragalactic Database (NED). [b] Heliocentric redshifts are as given in NED or if not listed in NED, as determined through host galaxy emission lines in visual-wavelength spectra of the SN. Measurements made by the authors are indicated with the † symbol. [c] References/URLs: LOSS (see Filippenko 2005, and references therein); Puckett (http://www.cometwatch.com); SDSS-II SN survey (Frieman et al. 2008); SNFactory (http://snfactory.lbl.gov/); CHASE (http://www.das.uchile.cl/proyectoCHASE/). [d] ‡: Obtained from the relation shown in Fig. 3 of Taddia et al. (2018).

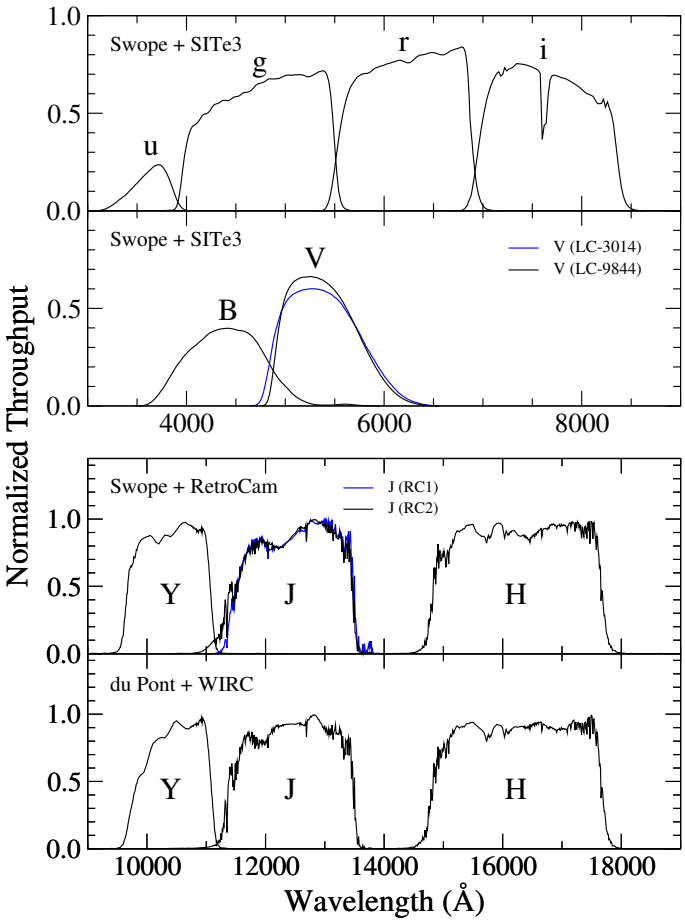

Fig. 2. CSP-I optical (*top panel*) and NIR (*bottom panel*) system response (telescope+detector+filters) functions for the Swope (+SITe3 and +RetroCam) and du Pont (+WIRC) telescopes. The normalized response functions include multiplications by an atmospheric transmission function for an airmass of 1.2 and telluric absorption spectrum appropriate to LCO.

functions have been multiplied by an atmospheric transmission function for an airmass of 1.2 and a telluric absorption spectrum appropriate to LCO. The optical response functions correspond to the filter set used with the Swope (+SITe3) telescope, and as described in Stritzinger et al. (2011), the original V-band filter ("$LV-3014$") broke on 14 January 2006 UT and was replaced with a similar V-band filter ("$LV-9844$") on 25 January 2006 UT. From our photometric calibration program it has been determined that the same color term applies to transform natural $LV-3014$ and $LV-9844$ system photometry to the standard Landolt V-band photometric system, and therefore any differences in photometry obtained with the passbands is well below 1%.

Turning to the NIR, the YJH-band system response functions shown in Fig. 2 correspond to filter sets installed in RetroCam and WIRC. Inspection of the RetroCam and WIRC system response functions reveals good agreement between their J and H throughputs, respectively, while clear differences are apparent between the two Y system response functions (see Krisciunas et al. 2017, for details). The Y-band was originally introduced by Hillenbrand et al. (2002) and is calibrated relative to Y-band magnitudes of the Persson et al. (1998) standard stars. The Y magnitudes of the Persson et al. standards are computed using $(Y-K_s)$ and $(J-K_s)$ color relations derived from a grid of Kurucz synthetic stellar atmosphere models with the added requirement that $(Y-K_s)=0$ when $(J-K_s)=0$ Krisciunas et al. (2017). This stipulation is an agreement with the primary standard star Vega being characterized by definition with zero magnitude in the JHK_s bands (Elias et al. 1982).

Finally, inspection of Fig. 2 also reveals that two J-band filters were used with RetroCam. As discussed in Krisciunas et al., the J_{RC1} filter experienced contamination issues in early 2009 and was replaced on 15 January 2009 with a new filter called, J_{RC2}, which was used throughout the remainder of the CSP-I (mid-2009). From our photometric calibration program we found the color term required to transform J_{RC1} and J_{RC2} magnitudes to the Persson et al. standard photometric system are discrepant enough to warrant two different J-band Swope (+RetroCam) natural systems. The difference in the color term computed for the J_{RC1} and J_{RC1} system response functions implies differences in SN photometry of 2% or less.

4. Observations and data reduction

A detailed description of the observing methodology and facilities at LCO used by the CSP-I is provided by Hamuy et al. (2006), while a thorough account of the data-reduction techniques including (i) the full processing of science and host-galaxy template images; (ii) subtraction of the host templates from each science image; (iii) construction of local sequences; and (iv) subsequent computation of definitive photometry is presented by Contreras et al. (2010) and Stritzinger et al. (2011).

All science images, host-galaxy templates, and standard-star fields were reduced in the conventional manner as described by Stritzinger et al. (2011, and references therein). Optical host-galaxy template images were obtained with the same filter set as the science images, in most cases with the du Pont telescope equipped with either facility Tek-5 or SITe2 CCD cameras, or occasionally with the Swope (+SITe3) telescope. All NIR template images were taken with the du Pont (+WIRC) telescope. Templates deemed suitable for galaxy subtraction were those in which the SN had sufficiently faded such that it was below our detection threshold, and were of excellent image quality, i.e., their seeing conditions are equal or superior to the science images. Once template subtraction was performed on each of the science images, photometry of the local sequence and SN was computed.

SN photometry was computed differentially with reference to a sequence of local standards calibrated with respect to standard star fields typically observed over a minimum of three photometric nights (see Krisciunas et al. 2017, for details). Definitive photometry of the local sequences in the standard Smith et al. (2002, *ugri*), Landolt (1992, *BV*), and Persson et al. (1998, *YJH*) photometric systems is listed in Tables 2 and 3, respectively. The quoted uncertainties accompanying the magnitudes of each of the local sequence stars correspond to the weighted average of the instrumental errors computed from measurements obtained over the course of multiple photometric nights.

Although the local sequences are reported in the standard systems as a service to the community, the CSP-I has a long tradition of publishing SN photometry in the natural photometric system. Photometry in the natural system is the purest form of the data, and allows us to avoid the notorious problem associated with using color terms derived from standard stars to transform SN photometry to the standard photometric system (Suntzeff 2000). To compute natural system SN photometry therefore requires us to construct catalogs of each of the local sequences that correspond to our various natural systems (i.e., Swope+SITe3, Swope+RetroCam, and du Pont+WIRC). To do this the standard

system photometry of the local sequences is placed on the natural system using transformation equations and color terms provided in Krisciunas et al. (2017). As mentioned above we have reason to believe the du Pont+Tek5 natural system is equivalent to the Swope+Site3 natural system.

Armed with local sequence photometry on the natural system, we proceeded to compute PSF photometry of the CSP-I SE SNe. Definitive natural system optical photometry of the SN sample obtained with the Swope and du Pont telescopes is listed in Tables 4 and 5, respectively. Definitive NIR photometry of the SN sample in the Swope natural system is given in Tables 6 and 7, where the former table contains $J_{\rm RC1}$ photometry and the later table contains $J_{\rm RC2}$ photometry. Finally, natural system NIR photometry obtained with the du Pont (+WIRC) telescope is listed in Table 8.

Reported along with each photometric measurement is a photometric error obtained by adding in quadrature the instrumental error of each SN photometry measurement with the nightly zero-point error. By electing to publish photometry on the natural system, the CSP-I data can be readily and accurately transformed to any user-defined photometric system through the use of S-corrections (Stritzinger et al. 2002). Finally, we note that all of the photometry presented in this paper is also available in electronic format on the CSP-I webpage.

5. Final light curves

The total number of photometry points contained within the CSP-I SE SN sample amounts to 2075 in the optical (u, 217 epochs; g, 357; r, 366; i, 376; B, 367; V, 391) and 468 in the NIR (Y, 165; J, 162; H, 141). Definitive light curves of the 34 CSP-I SE SNe are plotted in Fig. A.2. Overplotted on each of the light curves are Gaussian Process spline fits (dashed lines) computed within the SNooPy environment (Burns et al. 2011). The SNooPy fits provide an estimate of the peak magnitudes and the time of maximum brightness, along with robust uncertainties estimated via Monte Carlo simulations. For those objects with observations beginning past maximum, an estimate of the time of B-band maximum was obtained using the relation of Fig. 3 from Taddia et al. (2018). The relation correlates the time of B-band maximum to the time of maximum of the other passbands, all of which except the u band peak at phases after the time of B-band maximum. In these cases, the peak of the light curve was covered in at least one of the redder bands. Epochs of B-band maximum are listed in Table 1. Twenty of the 34 objects are found to have pre-maximum B-band light-curve coverage, with 12 of these having observations beginning at least five days prior to the time of B-band maximum. Furthermore, of the 26 objects with NIR follow-up observations, 17 have photometric measurements obtained before J-band maximum, and a subset of 14 have NIR coverage beginning at least 5 days earlier.

6. Prospects for the future

We have presented the definitive optical and NIR photometry of an expanded sample of well-observed SE SNe. The high-quality and dense photometric coverage for many of the objects within this data release, extending over eight filters, is particularly well-suited for tackling the problem of estimating host-galaxy extinction. In a companion paper (Stritzinger et al. 2018), the present observations are used to devise improved methods to estimate host-galaxy reddening. This is accomplished through the construction of intrinsic color-curve templates allowing for the inference of optical and NIR color excesses, the host reddening, $A_V^{\rm host}$, and (in some instances) the reddening-law parameter $R_V^{\rm host}$.

Armed with accurate estimates of host reddening, the CSP-I photometry sample is studied in detail in an additional companion paper by Taddia et al. (2018). This includes the analysis of the light-curve properties and luminosities, the construction of light-curve templates, and UVOIR bolometric light curves. The bolometric light curves are modeled with both semi-analytical and hydrodynamical modeling methods in order to constrain key explosion parameters (e.g., the ^{56}Ni abundance, the ejecta mass, and the explosion energy). Finally, the accompanying visual-wavelength spectroscopy of this sample is presented and studied in detail in a third companion paper by Holmbo et al. (in prep.).

Since the completion of the CSP-I follow-up program, we performed a second stage named the Carnegie Supernova Project II (CSP-II; 2011–2015). The main goal of CSP-II was to achieve the most accurate rest-frame NIR Hubble diagram by pushing the accuracy of Type Ia SN distances to the 1–2% level. However, observations of many young SNe of various types were also obtained, including more than a dozen SE SNe discovered prior to maximum brightness. The CSP-II SE SN sample is distinguished from others by our concerted efforts to build a large dataset of multi-epoch NIR spectroscopy. These data will offer a new avenue to study helium and hydrogen signatures in SE SNe, and ultimately will enable us to better understand the nature of such cosmic explosions.

We end with a few words on the future study of young SE SNe. In light of current and upcoming surveys such as the All-Sky Automated Survey for Supernovae (ASAS-SN; Shappee et al. 2014; Kochanek et al. 2017), the Asteroid Terrestrial-impact Last Alert System (ATLAS; Tonry 2011; Tonry et al. 2016), the Distance Less Than 40 Mpc survey (DLT40; Tartaglia et al. 2017), Pan-STARRS1 (Magnier et al. 2013), and the Zwicky Transient Facility (ZTF; Smith et al. 2014), progressively more young SE SNe will be discovered within hours of explosion. These early discoveries, coupled with high-cadence spectroscopy at medium or high resolutions, offer the potential to provide new constraints on SE SN progenitors, their pre-SN history, and the reddening of light produced by circumstellar dust.

Acknowledgements. We thank the referee for their thorough review of this manuscript. This paper is dedicated to the memory of our dear colleague, Wojtek Krzeminski (1933–2017), who played an important role in the early history of Las Campanas Observatory and who, during his retirement, obtained many of the observations presented in this paper. Special thanks to the technical staff and telescope operators of Las Campanas Observatory for their professional assistance over the course of the CSP-I, and also to James Hughes for providing invaluable maintenance for our computer network. M. D. Stritzinger, C. Contreras, and E. Hsiao acknowledge support provided by the Danish Agency for Science and Technology and Innovation realized through a Sapere Aude Level 2 grant and the Instrument-center for Danish Astrophysics (IDA). M. D. Stritzinger also acknowledges support by a research grant (13261) from the VILLUM FONDEN. M. D. Stritzinger conducted part of this research at the Aspen Center for Physics, which is supported by NSF grant PHY-1066293. M. Hamuy acknowledges support provided by the Millennium Center for Supernova Science through grant P10-064-F (funded by Programa Iniciativa Cientifica Milenio del Ministerio de Economia, Fomento y Turismo de Chile). This material is based upon work supported by the US National Science Foundation (NSF) under grants AST–0306969, AST–0607438, AST–0908886, AST–1008343, AST–1211916, AST–1613426, AST–1613455, and AST–1613472. A. V. Filippenko is also grateful for financial assistance from TABASGO Foundation, the Christopher R. Redlich Fund, and the Miller Institute for Basic Research in Science. The work of Filippenko was conducted in part at the Aspen Center for Physics, which is supported by NSF grant PHY–1607611; he thanks the Center for its hospitality during the neutron stars workshop in June and July 2017. This research has made use of the NASA/IPAC Extragalactic Database (NED), which is operated by the Jet Propulsion Laboratory, California Institute of Technology, under contract with the National Aeronautics and Space Administration.

References

Aldering, G., Humphreys, R. M., & Richmond, M. 1994, AJ, 107, 662
Anderson, J. P., Covarrubias, R. A., James, P. A., et al. 2010, MNRAS, 407, 2660
Anderson, J. P., Habergham, S. M., Jampes, P. A., et al. 2012, MNRAS, 424, 1372
Anupama, N., Sahu, D. K., Deng., J., et al. 2005, ApJ, 631, L125
Arcavi, I., Gal-Yam, A., Kasliwal, M. M., et al. 2010, ApJ, 721, 777
Arcavi, I., Gal-Yam, A., Yaron, O., et al. 2011, ApJ, 742, L18
Arcavi, I., Hosseinzadeh, G., Brown, P. J., et al. 2017, ApJ, 837, L2
Benvenuto, O. G., Bersten, M. C., & Nomoto, K. 2013, ApJ, 762, 74
Bersten, M. C., Benvenuto, O., & Nomoto, K. 2012, ApJ, 767, 143
Bersten, M., Tanaka, M., Tominaga, N., et al. 2013, ApJ, 767, 143
Bianco, F. B., Modjaz, M., Hicken, M., et al. 2014, ApJS, 213, 19
Blondin, S., & Tonry, J. L. 2007, ApJ, 666, 1024
Bufano, F., Pignata, G., Bersten, M., et al. 2014, MNRAS, 439, 1807
Burns, C. R., Stritzinger, M. D., Phillips, M. M., et al. 2011, AJ, 141, 19
Cano, Z. 2013, MNRAS, 434, 1098
Cao, Y., Kasliwal, M. M., Arcavi, I., et al. 2013, ApJ, 775, L7
Chevalier, R. A., & Fransson, C. 2008, ApJ, 683, L135
Chornock, R., Filippenko, A. V., Li., W., et al. 2011, ApJ, 739, 41
Cohen, J. G., Darling, J., & Porter, A. 1995, AJ, 110, 308
Contreras, C., Hamuy, M., Phillips, M. M., et al. 2007, AJ, 139, 519
Crockett, R. M., Eldridge, J. J., Smartt, S. J., et al. 2008, MNRAS, 391, L5
Drout, M. R., Soderberg, A. M., Avishay, G. Y., et al. 2011, ApJ, 741, 97
Eldridge, J. J., & Maund, J. R. 2016, MNRAS, 461, L117
Eldridge, J. J., Morgan, F., Smartt, S. J. et al. 2013, MNRAS, 436, 774
Elias, J. H., Frogel, J. A., Matthews, K., & Neugebauer, G. 1982, AJ, 87, 1029
Ergon, M., Sollerman, J., Fraser, M., et al. 2014, A&A, 562, A17
Filippenko, A. V. 1988, AJ, 96, 1941
Filippenko, A. V. 1997, ARA&A, 35, 309
Filippenko, A. 2005, in The Fate of the Most Massive Stars, eds. R. Humphreys, & K. Stanek (San Francisco: ASP), 33
Filippenko, A. V., Matheson, T., & Ho, L. C. 1993, ApJ, 415, L103
Filippenko, A. V., Li, W. D., Treffers, R. R., & Modjaz, M. 2001, in Small-Telescope Astronomy on Global Scales, eds. W. P. Chen, C. Lemme, & B. Paczyński (San Francisco: ASP), ASP Conf. Ser., 246, 121
Filippenko, A. V., Chornock, R., Swift, B., et al. 2003, IAU Circ. No. 8159, 2
Folatelli, G., Contreras, C., Phillips, M. M., et al. 2006, ApJ, 641, 1039
Folatelli, G., Bersten, M. C., Benvenuto, O. G., et al. 2014, ApJ, 793, L22
Folatelli, G., Van Dyk, S. D., Kuncarayakti, H., et al. 2016, ApJ, 825, L22
Foley, R. J., Papenkova, M. S., Swift, B. J., et al. 2003, PASP, 115, 1220
Fox, O. D., Bostroem, K. A., Van Dyk, S. D., et al. 2014, ApJ, 790, 17
Frieman, J., Bassett, B., Becker, A, et al. 2008, AJ, 135, 338
Galama, T. J., Vreeswijk, P. M., van Paradijis, J., et al. 1998, Nature, 395, 670
Galbany, L., Stanishev, V., Mourão, A. M., et al. 2016, A&A, 591, A48
Gal-Yam, A. 2016, ArXiv e-prints [arXiv:1611.09353]
Gal-Yam, A., Arcavi, I., Ofek, E. O., et al. 2014, Nature, 509, 471
Graur, O., Bianco, F. B., Huang, S., et al. 2017a, ApJ, 837, 120
Graur, O., Bianco, F. B., Modjaz, M., et al. 2017b, ApJ, 837, 121
Groh, J. H., Georgy, C., & Ekström, S. 2013, A&A, 558, L1
Hamuy, M., Folatelli, G., Morrell, N. I., et al. 2006, PASP, 118, 2
Hamuy, M., Deng., J., Mazzali, P. A., et al. 2009, ApJ, 703, 1612
Harkness, R. P., Wheeler, J. C., Margon, B., et al. 1987, ApJ, 317, 355
Hillenbrand, L. A., Foster, J. B., Persson, S. E., & Matthews, K. 2002, PASP, 114, 708
Hjorth, J., Sollerman, J., Møllerr, P. et al. 2003, Nature, 423, 847
Iwamoto, K., Mazzali, P. A., Nomoto, K., et al. 1998, Nature, 395, 672
Kawabata, K. S., Maeda, K., Nomoto, K., et al. 2010, Nature, 465, 326
Kochanek, C. S., Shappee, B. J., Stanek, K., et al. 2017, PASP, 129, 104502
Krisciunas, K., Contreras, C., Burns, C. R., et al. 2017, AJ, 154, 211
Kumar, B., Pandey, S. B., Sahu, D. K., et al. 2013, MNRAS, 431, 308
Landolt, A. U. 1992, AJ, 104, 340
Langer, N. 2012, ARA&A, 50, 107
Leloudas, G., Gallazzi, A., Sollerman, J., et al. 2011, A&A, 530, A95
Li, W. 2008, ATel, 1433, 1
Li, W., Leaman, J., Chornock, R., et al. 2011, MNRAS, 412, 1441
Liu, Y. Q., & Modjaz, M. 2014, ArXiv e-prints [arXiv:1405.1437]
Liu, Y. Q., Modjaz, M., & Bianco, F. B. 2017 ApJ, 845, 85
Lyman, J. D., Bersier, D., James, P. A., et al. 2016, MNRAS, 457, 328
Magnier, E. A., Schlafly, E., Finkbeiner, D., et al. 2013, ApJS, 205, 20
Matheson, T., Filippenko, A. V., Li, W., Leonard, D. C., & Shields, J. C. 2001, AJ, 121, 1648
Matheson, T., Garnavich, P. M., Stanek, K. Z., et al. 2003, ApJ, 599, 394
Maund, J. R., Smartt, S. J., Kudritzki, R. P., et al. 2004, Nature, 427, 129
Maund, J. R., Fraser, M., Ergon, M., et al. 2011, ApJ, 739, L37
Maund, J. R., Arcavi, I., Ergon, M., et al. 2015, MNRAS, 454, 2580
Mazzali, P. A., Deng, J., Maeda, K., et al. 2002, ApJ, 572, L61
Mazzali, P. A., Deng, J., Pian, E., et al. 2006, ApJ, 645, 1323
Mazzali, P. A., Deng, J., Hamuy, M., Nomoto, K., et al. 2009, ApJ, 703, 1624
Milisavljevic, D., Margutti, R., Soderberg, A. M., et al. 2012, ApJ, 767, 71
Modjaz, M., Kewley, L., Bloom, J. S., et al. 2011, ApJ, 731, L4
Modjaz, M., Liu, Y. Q., & Bianco, F. B. 2016, ApJ, 832, 108
Morales-Garoffolo, A., Elias-Rosa, N., Benetti, S., et al. 2014, MNRAS, 445, 1647
Nakar, E., & Piro, A. L. 2014, ApJ, 788, 193
Perets, H. B., Gal-Yam, A., Mazzali, P. A., et al. 2010, Nature, 465, 322
Persson, S. E., Murphy, D. C., Krzeminski, W., Roth, M., & Rieke, M. J. 1998, AJ, 116, 2475
Pettini, M., & Pagel, B. E. J. 2004, MNRAS, 348, 56
Pingata, G., Stritzinger, M., Soderberg, A. M., et al. 2011, ApJ, 728, 14
Piro, A. L. 2015, ApJ, 808, L51
Piro, A. L., Muhleisen, M. E., & Arcavi, I. 2017, ApJ, 846, 94
Prentice, S. J., & Mazzali, P. A. 2017, MNRAS, 469, 2672
Prentice, S. J., Mazzali, P. A., Pian, E., et al. 2016, MNRAS, 458, 2973
Puls, J., Vink, J. S., & Najarro, F. 2008, A&ARv, 16, 209
Rheault, J. P., DePoy, D. L., Behm, T. W., et al. 2010, Proc. SPIE, 7735, 773564
Richmond, M. W., Treffers, R. R., Filippenko, A. V., et al. 1994, AJ, 107, 1022
Sanders, N. E., Caldwell, N., McDowell, J., & Harding P. 2012, ApJ, 758, 133
Sapir, N., & Waxman, E. 2017, ApJ, 838, 130
Shappee, B., Prieto, J. L., Grupe, D., et al. 2014, ApJ, 788, 48
Shivvers, I., Groh, J., Mauerhan, J. C., et al. 2015, ApJ, 806, 213
Shivvers, I., Modjaz, M., Zheng, W., et al. 2017, PASP, 129, 054201
Smartt, S. J. 2009, ARA&A, 47, 63
Smith, N., & Owocki, S. P. 2006, ApJ, 645, L45
Smith, J. A., Tucker, D. L., Kent, S. et al. 2002, AJ, 123, 2121
Smith, N., Li, W., Filippenko, A. V., & Chornock, R. 2011, MNRAS, 412, 1522
Smith, R. M., Dekany, R. G., Bebek, C., et al. 2014, SPIE, 9147, 79
Soderberg, A. M., Margutti, R., Zauderer, B. A., et al. 2012, ApJ, 752, 78
Stanek, K. Z., Matheson, T., Garnavich, P. M., et al. 2003, ApJ, 591, L17
Stritzinger, M., Hamuy, M., Suntzeff, N. B., et al. 2002, AJ, 124, 2100
Stritzinger, M., Mazzali, P. A., Phillips, M. M., et al. 2009, ApJ, 696, 713
Stritzinger, M., Phillips, M. M., Boldt, L. N., et al. 2011, AJ, 142, 156
Stritzinger, M. D., Taddia, F., Bersten, M., et al. 2018, A&A, 609, A135 (Paper II)
Suntzeff, N. B. 2000, in Cosmic Explosions, eds. S. S. Holt, & W. W. Zhang (New York: AIP), 65
Swartz, D. A., Clocchiatti, A., Benjamin, R., Lester, D. F., & Wheeler, J. C. 1993, Nature, 365, 232
Taddia, F., Sollerman, J., Leloudas, G., et al. 2015, A&A, 574, A60
Taddia, F., Stritzinger, M., Bersten, M., et al. 2018, A&A, 609, A136 (Paper III)
Tartaglia, L., Fraser, M., Sand, D. J., et al. 2017, ApJ, 836, L12
Tominaga, N., Tanaka, M., Nomoto, K., et al. 2005, ApJ, 633, L97
Tonry, J. L. 2011, Phil. Trans. R. Soc. London, Ser. A, 371, 20120269
Tonry, J., Denneau, L., Stalder, B., et al. 2016, ATel, 9526, 1
van Driel, W., Yoshida, S., Nakada, Y., et al. 1993, PASJ, 45, L59
Van Dyk, S. D., Li, W., Cenko, S. B., et al. 2011, ApJ, 741, L28
Van Dyk, S. D., Zheng, W., Fox, O. D., et al. 2014, AJ, 147, 37
Vink, J. S. 2011, Ap&SS, 336, 163
Yaron, O., Perley, D. A., Gal-Yam, A., et al. 2017, Nat. Phys., 13, 510
Yoon, S. G. 2015, PASA, 32, 15
Yoon, S. C., & Cantiello, M. 2010, ApJ, 717, L62

Appendix A: Additional figures

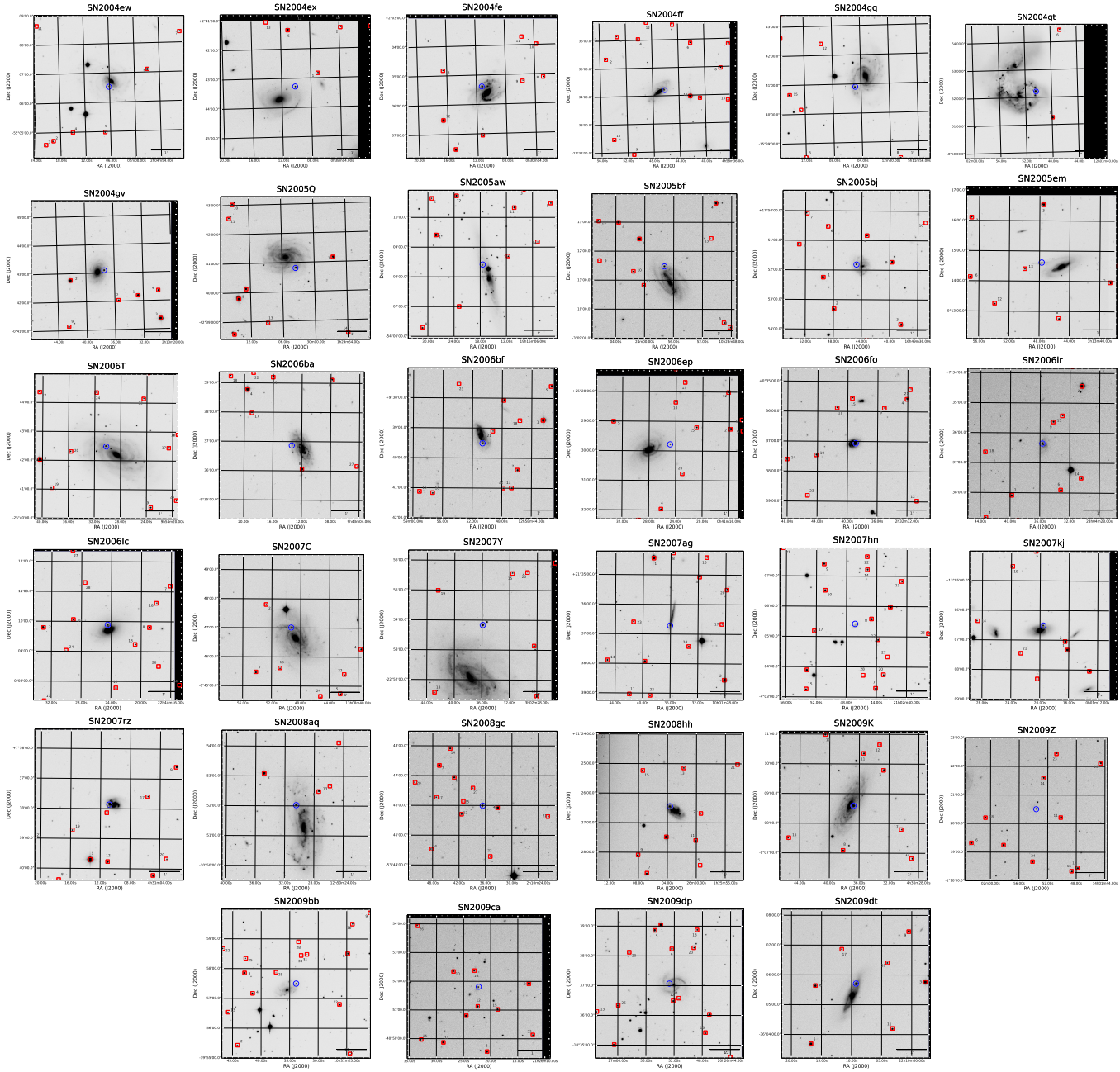

Fig. A.1. A mosaic of *V*-band CCD images of 34 SE SNe observed by the CSP-I. Each supernova is indicated with a blue circle, while optical local sequence stars are marked with red squares.

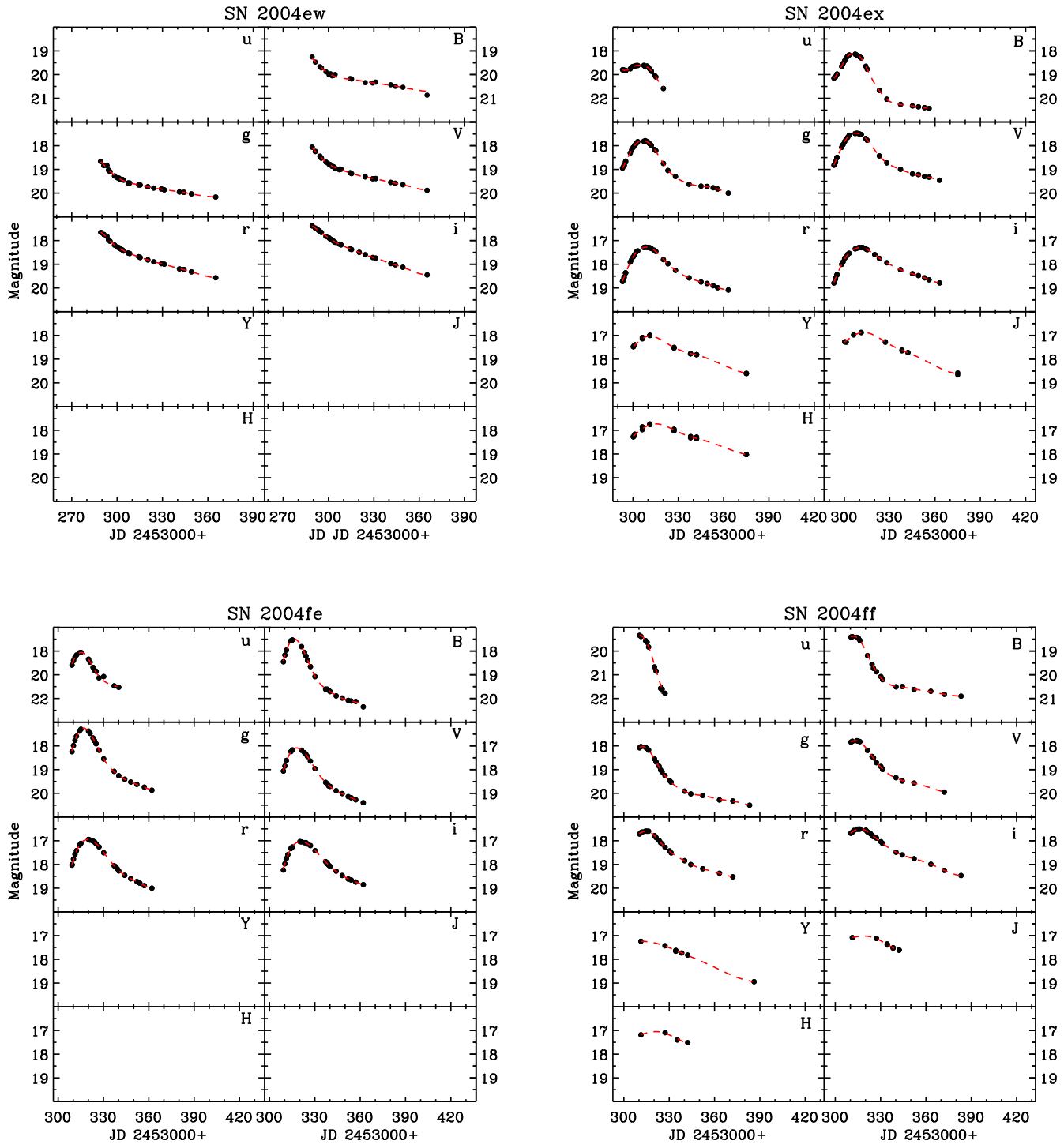

Fig. A.2. Light curves of CSP-I SE SNe in the Swope natural photometric system. Uncertainties in the photometry are smaller than the points, unless shown. The smooth curves correspond to Gaussian process spline fits computed within the light-curve analysis software package SNooPy (Burns et al. 2011).

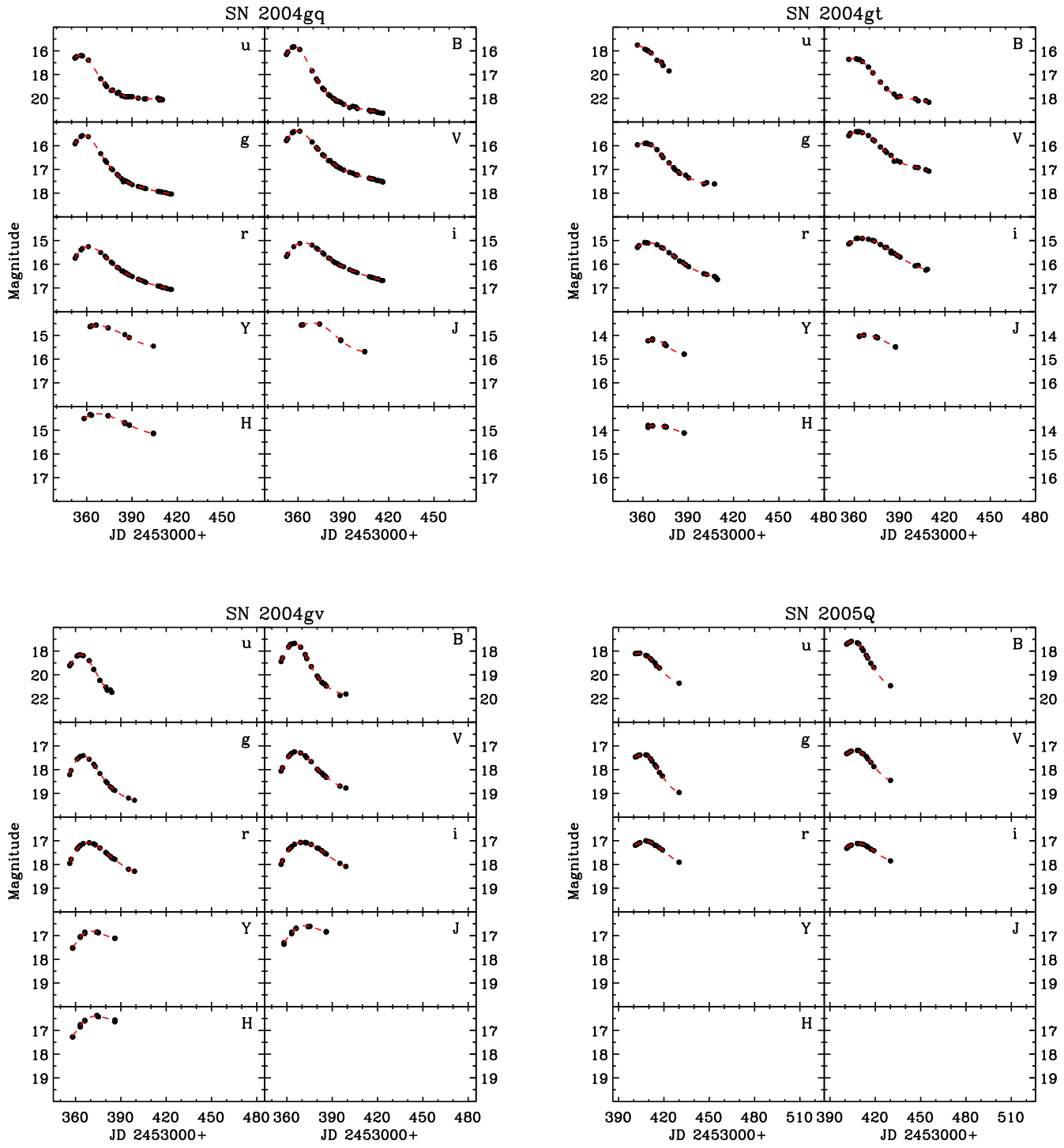

Fig. A.2. continued.

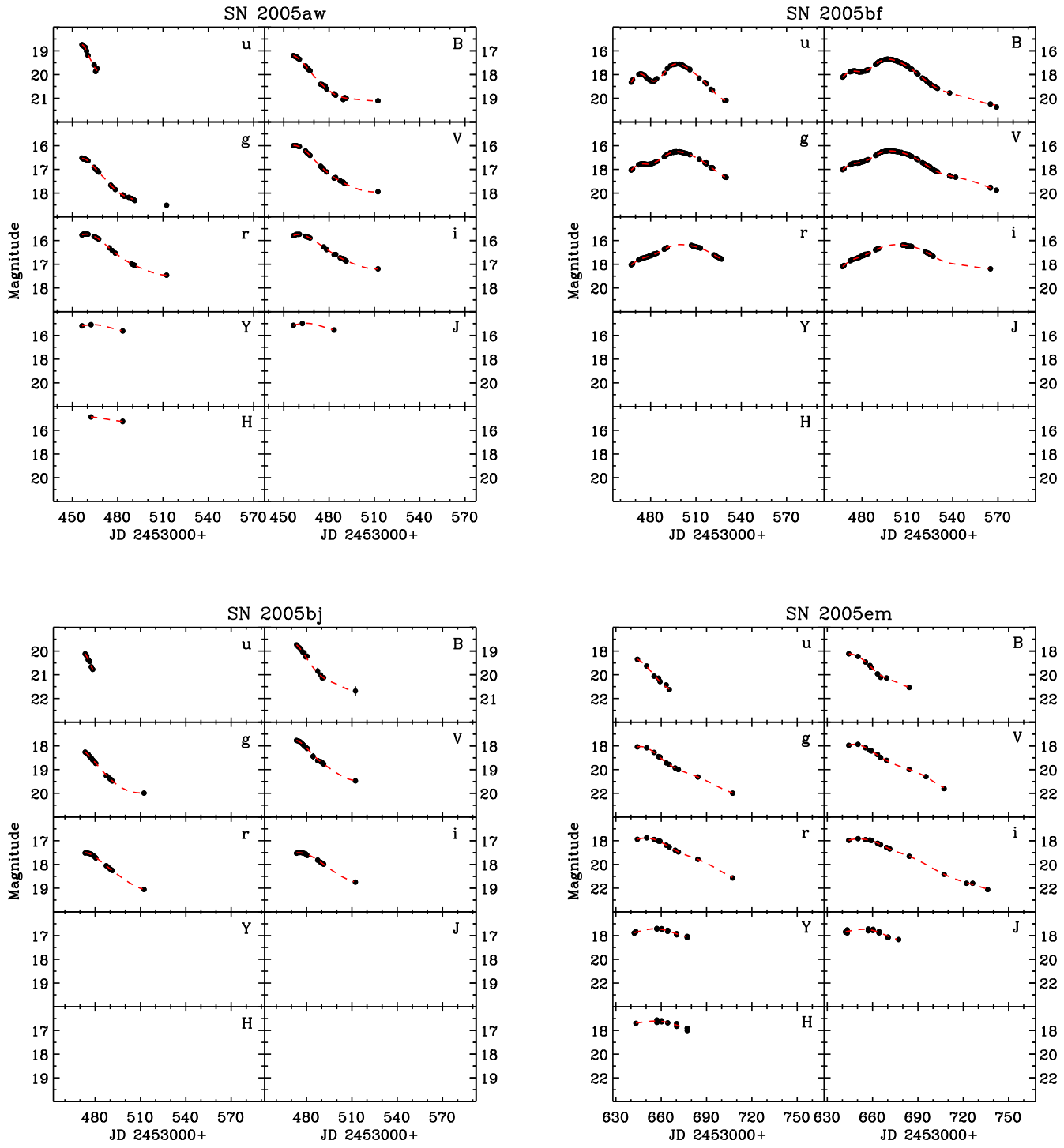

Fig. A.2. continued.

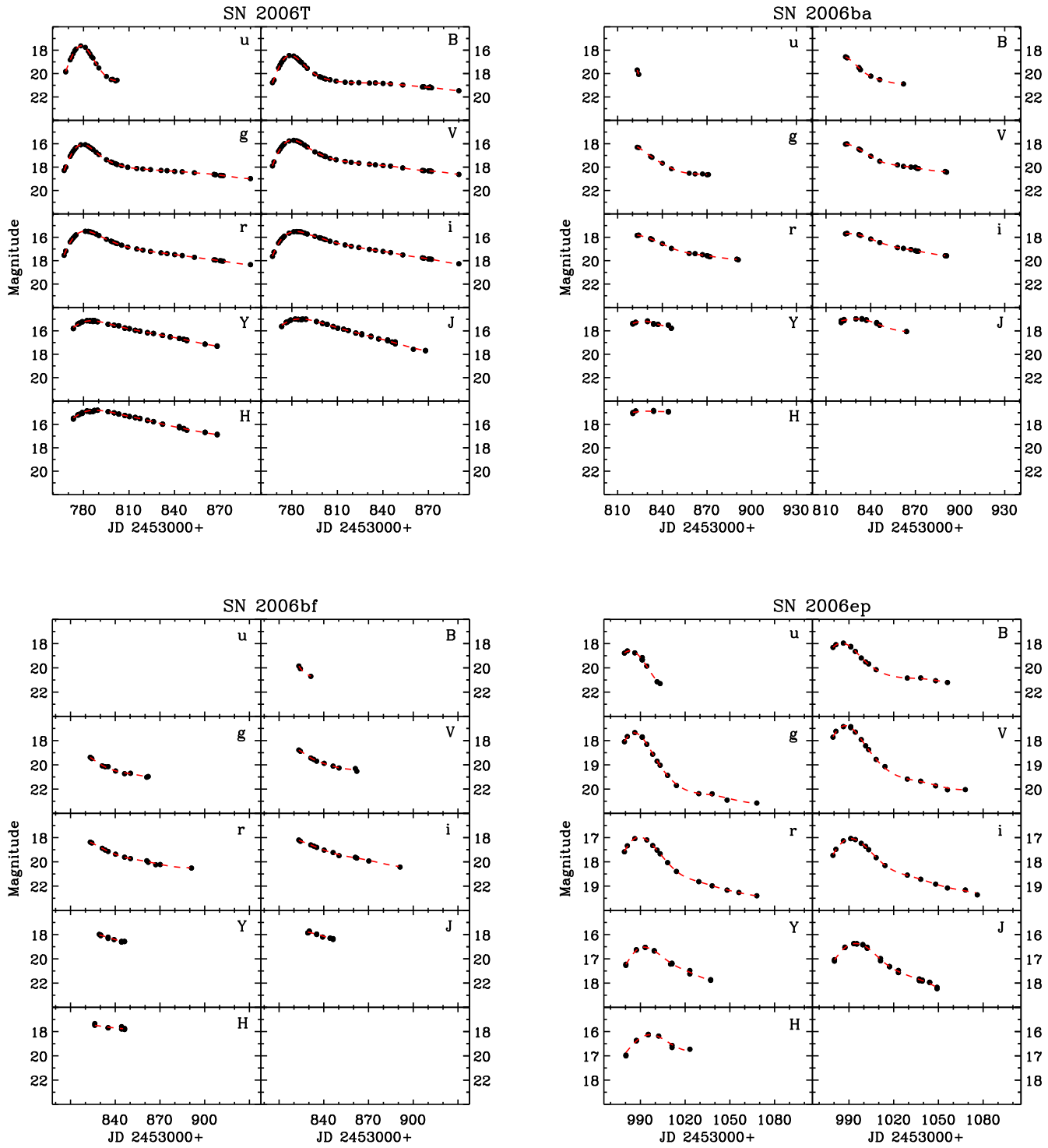

Fig. A.2. continued.

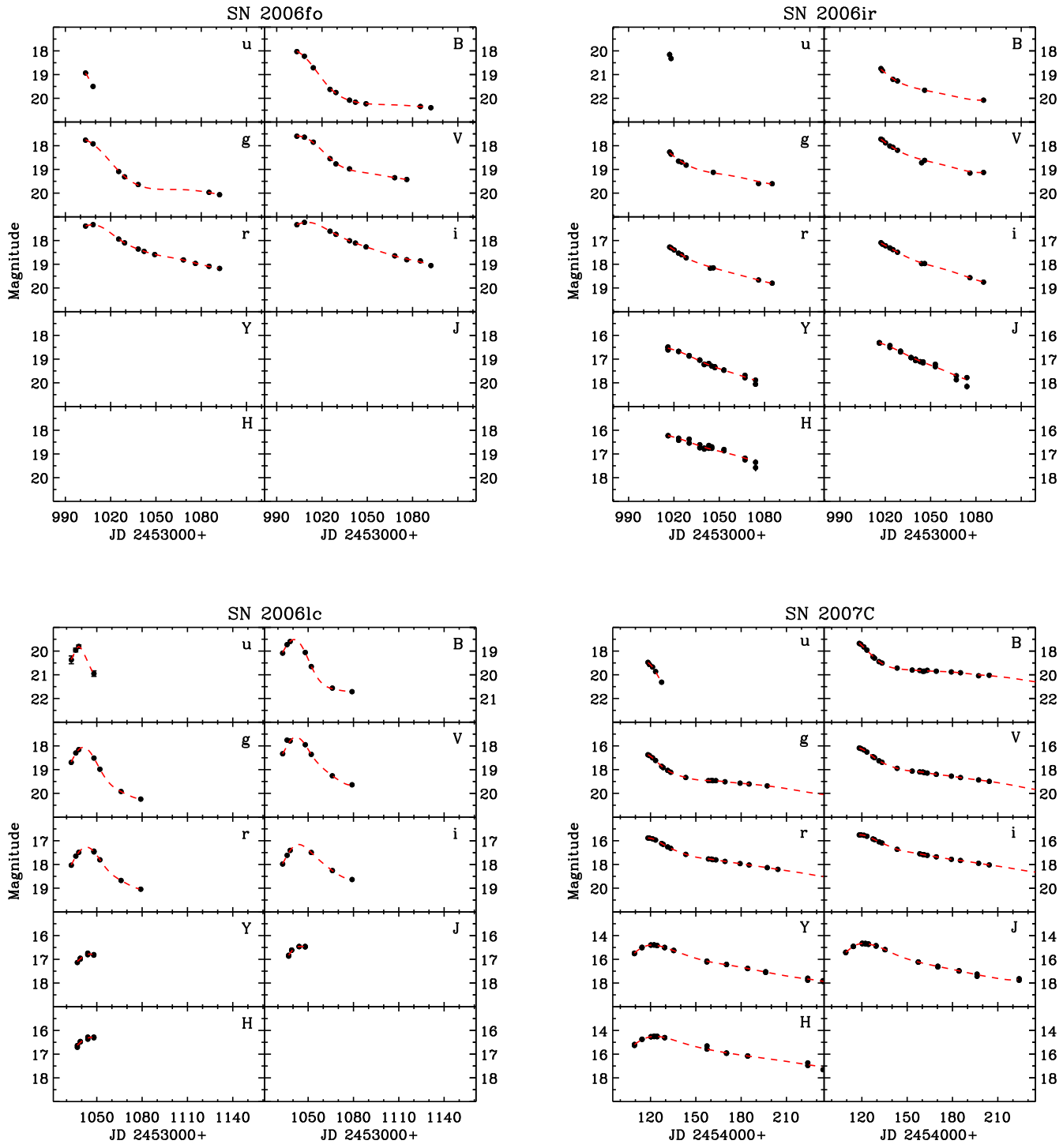

Fig. A.2. continued.

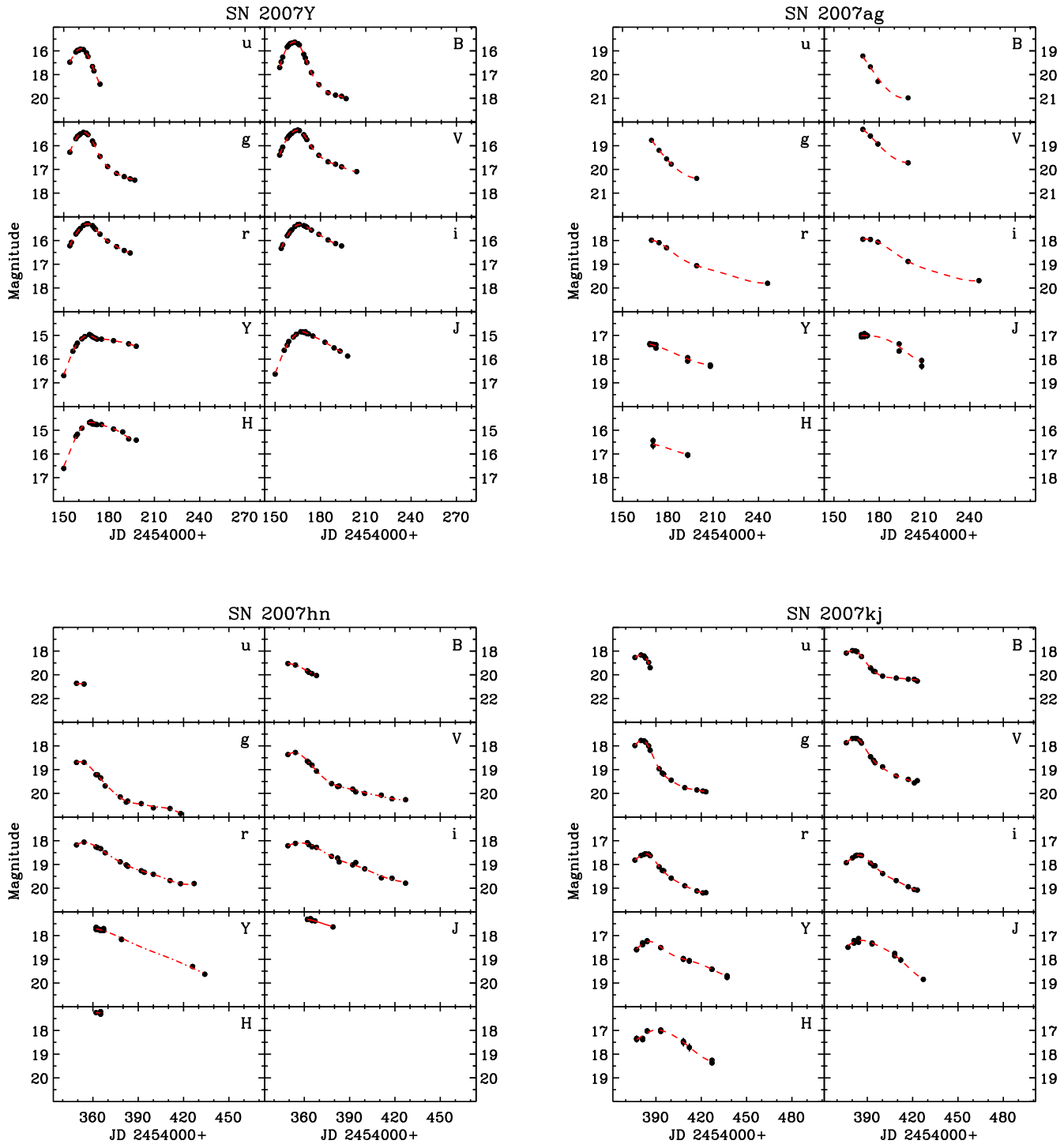

Fig. A.2. continued.

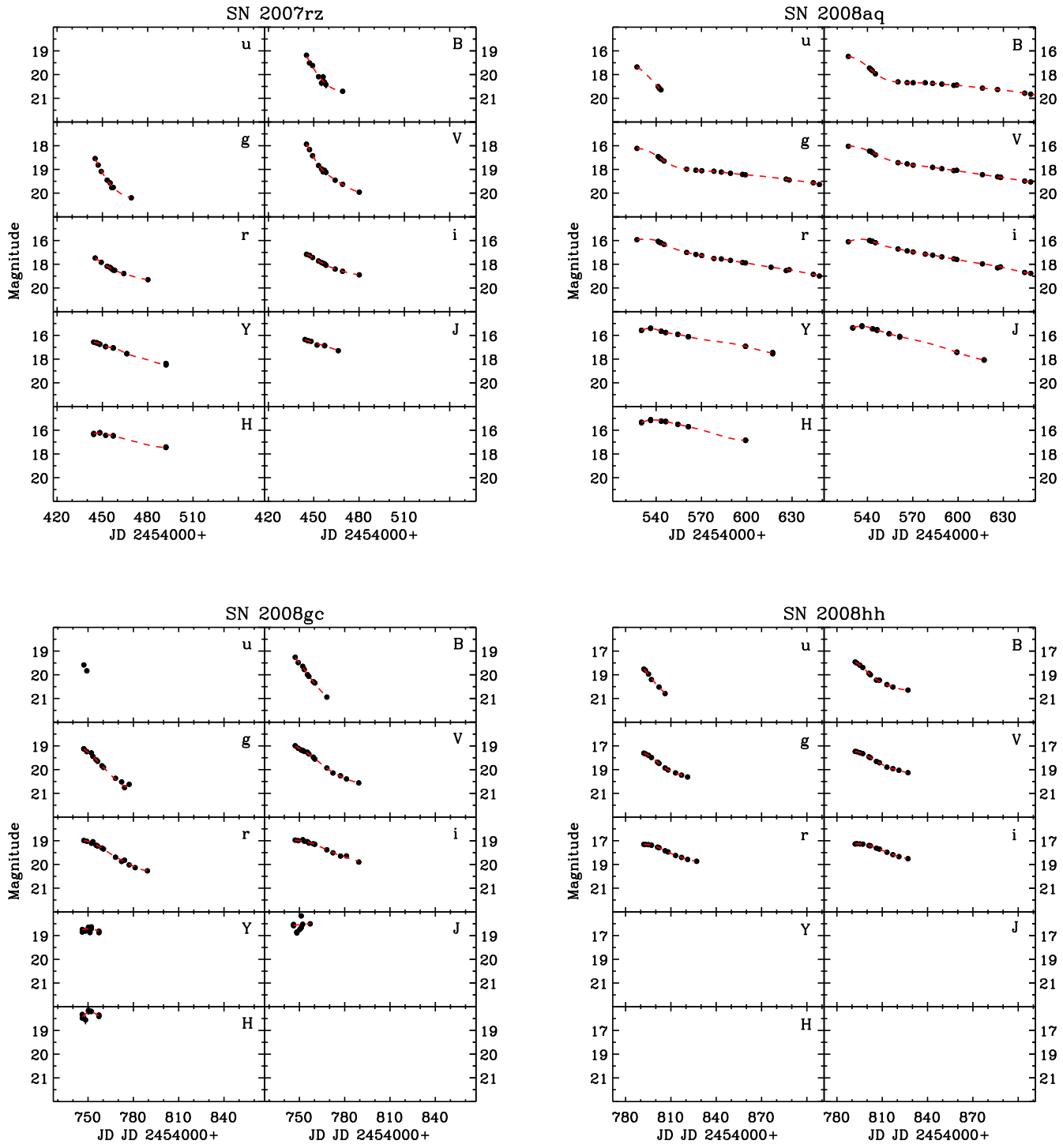

Fig. A.2. continued.

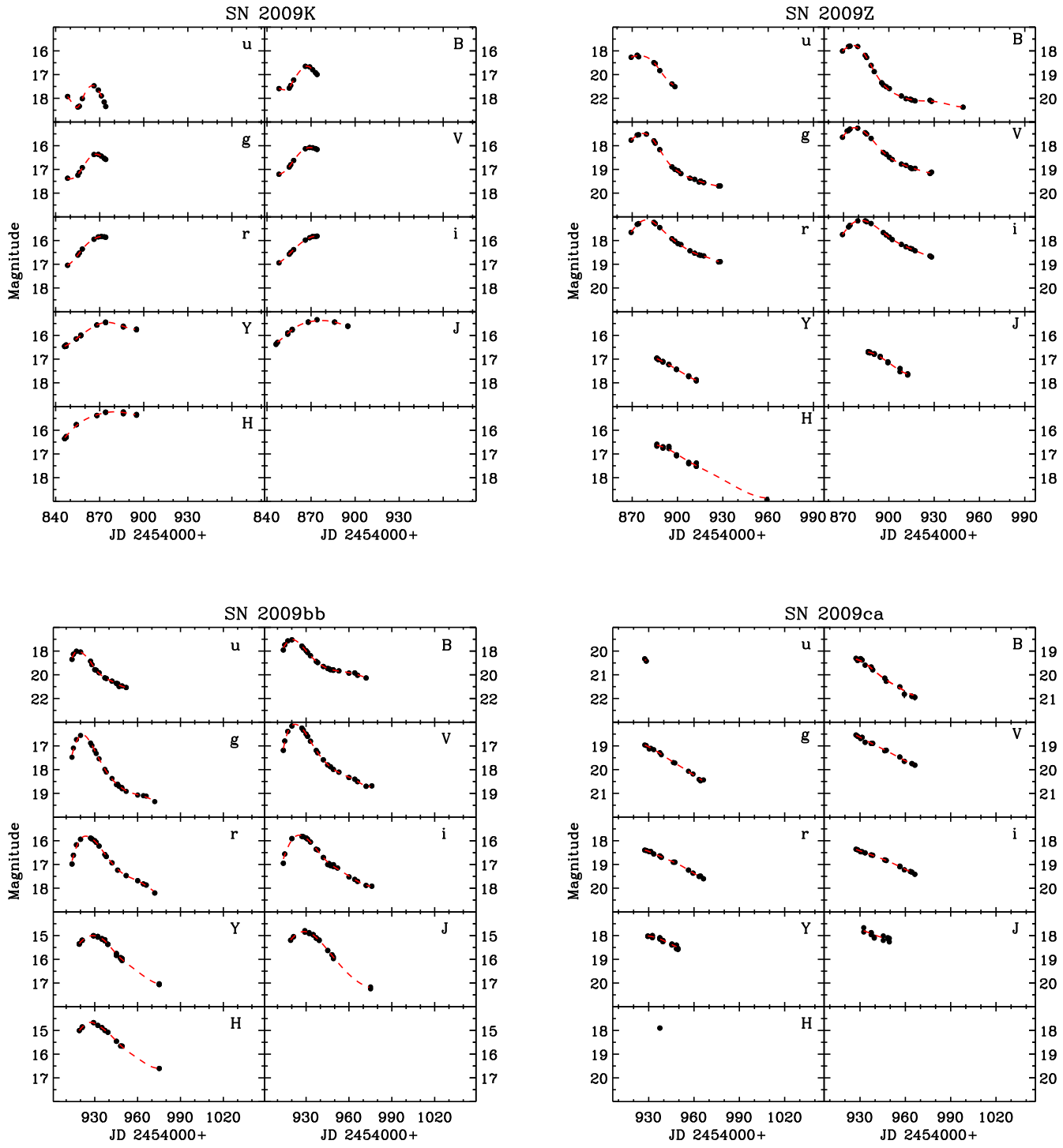

Fig. A.2. continued.

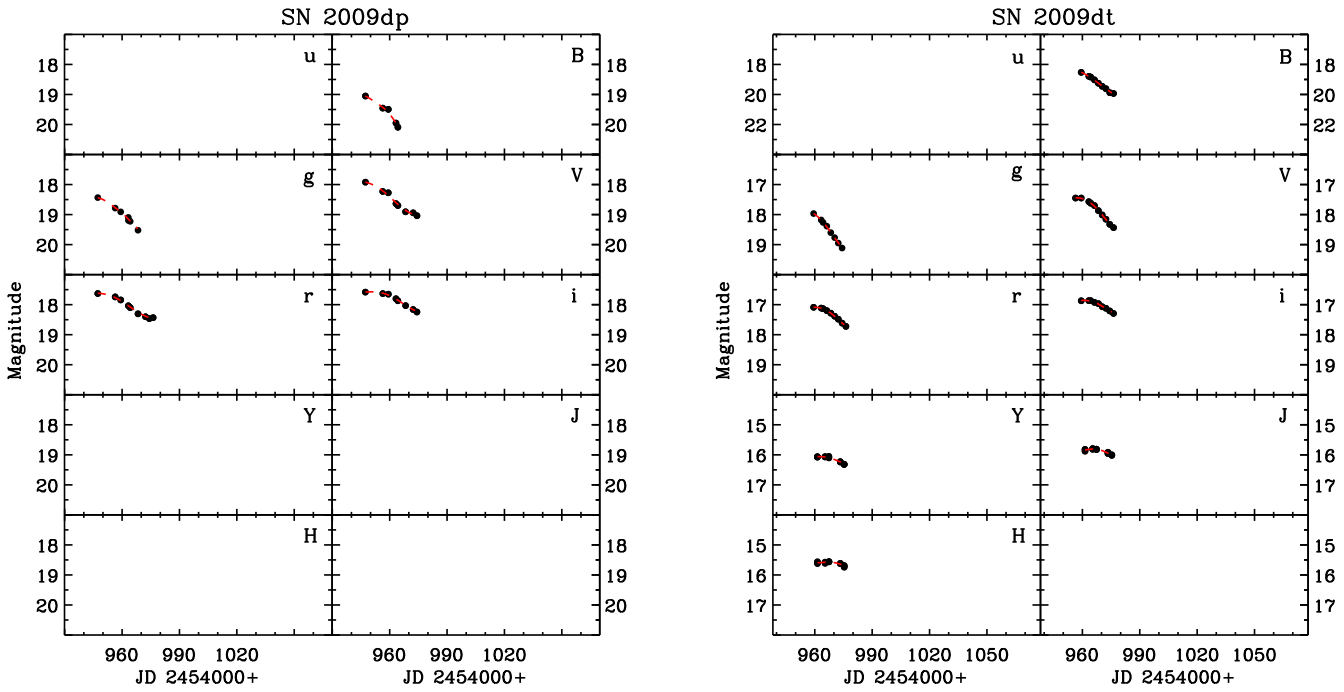

Fig. A.2. continued.